*Iraqi Journal of Physics, 2026*
*https://doi.org/10.30723/ijp.v24i2.1428*

*Vol.24, No.2, PP.58-70*
*P-ISSN: 2070-4003*
*E-ISSN: 2664-5548*

# Influence of Dual Zn and Sn Ions Doping on the Properties of Electrospun PVP Fibers for Photodetector-Photosensor Applications

**Yasser O. Naif [1*] and Isam M. Ibrahim[1]**
[1]*Department of Physics, College of Science, University of Baghdad, Baghdad, Iraq*
[*]Corresponding author: yasir.udah2404m@sc.uobaghdad.edu.iq

## Abstract
In this study, polyvinylpyrrolidone (PVP) fibers were fabricated using electrospinning, and their properties were enhanced through dual doping with zinc (Zn) and tin (Sn) ions at different Zn: Sn mixing ratios. The structural, optical, and electrical characteristics of the fibers were investigated to evaluate their potential for photodetector applications. The X-ray diffraction (XRD) analysis of pure PVP fibers indicates an amorphous nature, whereas two broad diffraction peaks emerge after mixing with ions, which is caused by the rearrangement of PVP chains due to their interactions with the added ions. Field emission scanning electron microscope (FESEM) images show a significant reduction in fiber diameters and an increase in the density of the prepared fabric with an increase in the metal ion dopant. Fourier transform Infrared (FTIR) analysis revealed shifts and intensity changes in characteristic peaks and the appearance of metal oxide bands, indicating interactions between the polymer matrix and the dopant ions, that contributing to the enhanced functional properties. Incorporating Zn and Sn ions significantly improved the photodetector performance of PVP fiber/n-Si devices. The doping with the two ions significantly enhanced the photocurrent to 12.5 times compared to 2.5 times in the pure PVP fiber/n-Si sample. The fabricated photodetector fibers at a 3:7 metal ion to PVP ratio show a maximum photosensitivity of 24.8% under a violet light source. The results from this study demonstrate the potential of dual Zn and Sn ion-doped PVP fibers as efficient, low-cost, and flexible materials for photodetector applications to violet light.

**Article Info.**

**Keywords:**
*PVP Fiber, Electrospinning, Photodetector, Structural Properties, Optical Properties.*

**Article history:**
*Received: Jan. 30, 2025*
*Revised: May, 06, 2025*
*Accepted:May, 18, 2025*
*Published:Jun. 01,2026*

## 1. Introduction
Electrospun fibers have gained significant attention due to their unique properties, including high surface area-to-volume ratio, tunable porosity, and mechanical flexibility [1]. These characteristics make electrospinning fibers suitable for a wide range of applications, including air or water filtration [2], tissue engineering [3], gas sensors [4], and detectors [5]. By adjusting various processing parameters, the electrospinning technique can produce fibers with controllable properties, such as diameter, shape, distribution, and orientation [6]. The working parameters of electrospun fibers include solution viscosity, applied voltage, flow rate, and the needle-collector distance [7]. Additionally, incorporating functional dopants, such as metal ions or nanoparticles, further enhances the properties of the fibers, enabling them for specific applications [8]. Varying the type, concentration, and combination of dopants [9]. It is possible to tailor the mechanical, thermal, optical, magnetic, and electrical properties [10,11].

Conventional photodetectors are typically fabricated based on silicon, germanium, or other inorganic semiconductors due to their excellent optoelectronic properties [12]. However, these materials often involve complex and costly fabrication processes, limited flexibility, and poor compatibility [13]. Recently, polymer-based composite materials have emerged as a promising alternative for photodetector applications [14]. Electrospun polymer composite fibers combine polymers' flexibility and low cost with the enhanced functional properties of incorporated dopants, such as metal ions or nanoparticles [15].

Incorporating metal ions into the electrospun polyvinylpyrrolidone (PVP) fiber matrix enhances the performance of the fabricated detectors. These metal ions can interact with the

polymeric chains and influence the local electronic environment, potentially reduction the energy band gap by introducing localized states within the band structure. Furthermore, their presence can enhance the generation and mobility of charge carriers, which is essential for improving the sensitivity and overall performance of the detectors [16].

Jilani et al. (2024) [17] examined composite materials based on polyvinyl alcohol (PVA)/PVP blend loaded by CdS/ZnO core–shell nanostructures. The resulted nanocomposites exhibited improved functional properties, such as enhanced electrical conductivity and optical transparency. Hamadamin et al. (2025) [18] prepared $Cr_2O_3$-doped PVP nanofibers with high crystallinity and UV light sensitivity onto glass substrates by electrospun deposition at room temperature.

This study focuses on fabricating and characterizing electrospun PVP fibers doped with Zn and Sn ions. The goal is to investigate how dual ion doping influences the structural and functional properties of the fibers and to evaluate their potential in photodetector applications.

## 2. Experimental Setup

The starting materials are PVP of MW~9000 (from Sigma-Aldrich), tin acetate ($Sn(CH_3CO_2)_2$), and zinc acetate ($Zn(CH_3CO_2)_2$) from Sigma-Aldrich Co. 1 g of PVP was dissolved in 12 mL of 70% ethanol: water solution under stirring for 6 hours at room temperature. 0.5 g of each tin and zinc acetate was dissolved in 10 mL of an ethanol: water solution. The metal acetate solutions at different mixing volumetric (Sn, Zn) to PVP ratios of 0:10, 1:9, 2:8, and 3:7 were mixed with the PVP solution by a magnetic stirrer for 40 minutes.

The flow rate of polymer injection by syringe pump was fixed at 0.5 mL/h. The needle-to-collector separation distance was adjusted to 12 cm. A voltage difference of 20 kV was applied, where the syringe was connected to the positive pole of the power supply and the collector to the negative pole, as shown schematically in Fig. 1. The electrospun doped PVP fibers were deposited on glass substrates.

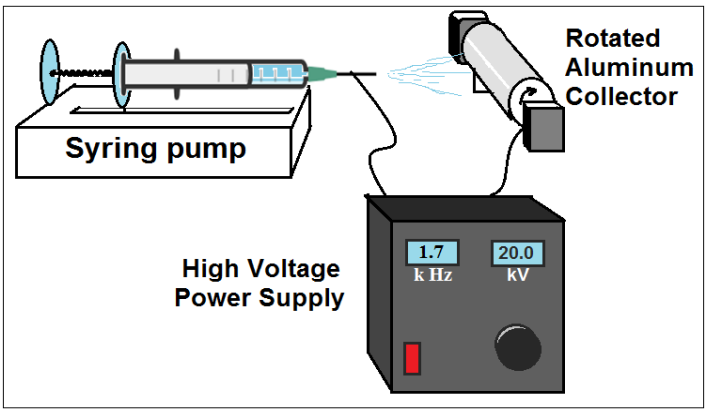


***Figure 1: Electrospun experimental setup.***

The surface morphology and crystallinity of pure and doped electrospun PVP fibers were examined by a field emission scanning electron microscope (FESEM) (Inspect f-50) and X-Ray diffractometer (XRD) (Shimadzu 6000). The Fourier transformer Infrared spectroscopy (FTIR) from Shimadzu was used to identify chemical bonds and functional groups in the prepared samples.

Fig. 2 shows the scheme of a photodetector based on an electrospun (Zn, Sn) ion-doped PVP fiber layer on an n-type Si. An aluminum mesh electrode of 200 nm thickness was thermally evaporated on the fiber layer surface with the aid of a suitable mask under a high vacuum using the Eduard coating system at room temperature. An aluminum electrode was deposited on the entire back of the Si wafer. Thin wire connections were attached to the Al electrodes by silver paste.

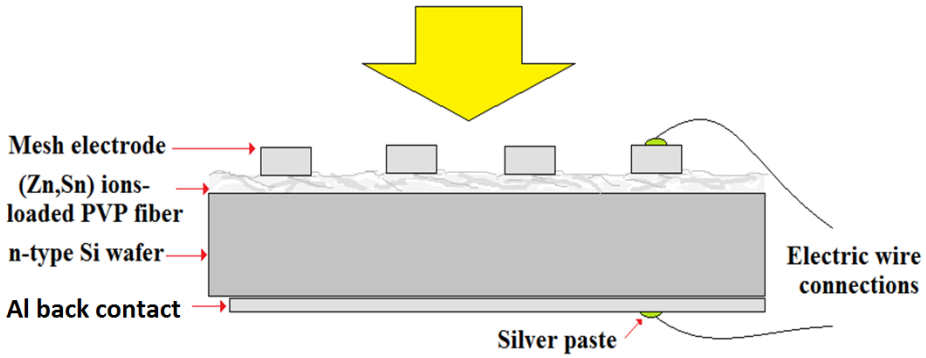


***Figure 2: Schematic diagram of the prepared photodetector.***

The photocurrent response was examined under light conditions using different light colors of 20 mW/cm$^2$ intensity. Photocurrent measurements were performed using a Keithley 2400 Source Meter to record the current variation under illumination at 1 V forward bias voltage.

## 3. Results and Discussion

Fig. 3 displays the XRD patterns of the electrospun PVP fiber on glass slides compared to those of the dual ions of Zn and Sn-doped electrospun PVP at different mixing ratios. The pure PVP fiber shows an amorphous nature. This result agrees with previous studies [19, 20]. No variations were noticed at low mixing ratios of the two ions, while at the 3:7 ratio, two broad diffraction peaks appeared at diffraction angles 2θ ≈ 14° and 17°. These two diffraction peaks result from more arrangements of PVP chains and the strengthening of their ordered structure, indicating its semi-crystalline nature, which was assigned to previous literature work (JCPDS card No. 65-2870) [21]. These peaks reflect the short-range order in the polymer chains. These results agree with those reported by Hotaby et al. [22].

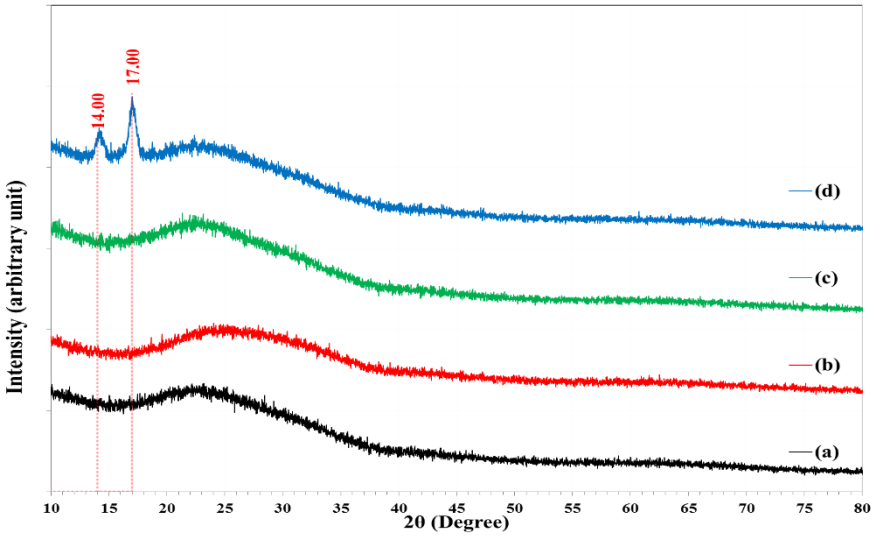


***Figure 3: XRD patterns of (a) the electrospun PVP fiber and that of the dual doped with Zn and Sn at different mixing ratios of (b) 1:9, (c) 2:8, and (d) 3:7.***

Fig. 4 displays the FESEM images of electrospun PVP fibers doped with zinc and tin at different mixing ratios. Variations in fibers diameter and distribution over the surface with increasing mixing ratio were noticed. The pristine PVP fibers have uniform fiber diameters of several microns in length distributed randomly. The histogram of fiber diameter next to the image, completed using SPSS software, displays a mean diameter of 179.4 nm, with standard deviation of 58 nm. The mixing of zinc and tin acetates at a 1:9 mixing ratio reduced the mean fiber diameter

to 142.47 nm, in addition to minor irregularities with a 71.59 nm standard deviation. The mixing ratio of 2:8 caused a significant reduction in fiber diameters to a mean value of 93.07 nm and a more systematic diameter. The electrospun PVP fiber film exhibited a higher number of crosslinking points. The fibers' diameter became thinner at the mixing ratio of 3:7. It became 71.55 nm, with a narrow distribution; a dense fabric appeared in this ratio. The fibers at this ratio appeared dotted, probably due to the accumulation of added ions on the fiber surface. These variations in fiber morphology agree with the study of Nartetamrongsutt and Chase [23]. The significant reduction of fiber diameter, especially at a high mixing ratio, may be due to the decrease in viscosity of the polymer blend during extrusion in the deposition process. These variations of fiber diameters and their distribution over the surface with increasing mixing ratios with the two ions convert it to denser, entangled fabric, improving the entire surface area of the fiber network and enhancing its capability for sensor applications.

The FTIR transmission spectra of the electrospun PVP fiber and that of the dual-doped with Zn and Sn at different mixing ratios are shown in Fig. 5. The pure sample displays several characteristic peaks of PVP structure and some bands corresponding to the moisture content. The broad absorption band centered at 3436 $cm^{-1}$ corresponds to the hydroxyl group (-OH). The two bands at 2923 and 2853 $cm^{-1}$ are attributed to the C-H asymmetric and symmetric stretching vibrations in the CH2 group [24], while their bending modes appeared at 1464 and 1425 $cm^{-1}$ [25]. The band at 1659 $cm^{-1}$ is assigned to the C=O stretching of the amide group in the PVP [26]. The band appears at 1290$cm^{-1}$ associated with C-N stretching, and at 1114 $cm^{-1}$, corresponding to C-O vibration [27].

After mixing with the two ions of Zn and Sn, slight variations in the spectra were observed in terms of band shift, intensity, and the emergence of metal oxide bands, due to the bonding between the added ions and the functional groups of the polymer. Increasing the mixing ratio causes the attendance of bands associated with Sn-O and Sn-O-Sn bonds to be more distinct at 650 and 586 $cm^{-1}$, respectively [28]. In addition, the appearance of the broad band around 490 $cm^{-1}$ corresponds to the Zn-O bond. These bands confirm the interaction of these ions with oxygen in the PVP structure [24]. The more predominant Zn-O than Sn-O bands result from the high degree of oxidation of zinc compared with tin. Table 1 lists the FTIR bands of electrospun PVP fibers mixed with Zn and Sn ions at different ratios.

Fig. 6 illustrates the UV-Visible absorbance spectra of the pure and doped electrospun PVP fiber with Zn and Sn ions at different mixing ratios deposited on glass substrates. The curves indicate that absorbance increases, particularly in the UV range, as the mixing ratio rises, accompanied by a slight redshift of the absorbance edge. These changes are attributed to the interactions between tin and zinc ions with the PVP matrix, leading to improved charge transfer and new localized electronic states. The higher absorbance in the UV range and reduction of the bandgap make the prepared fiber fabric layer promising for photoelectronic applications [29]. The Tauc plots are utilized to determine the energy gap $E_g^{Opt.}$ of pure and doped PVP fibers at different (Zn:Sn) ratios, Eq. (1) [30], as shown in Fig. 7.

$$(\alpha h\nu)^2 = B(h\nu - E_g^{Opt.}) \quad \textbf{(1)}$$

where α represents the absorption coefficient, $h\nu$ is the photon energy, and B is a constant.

The bandgap significantly decreased from 4.0 eV for the pure PVP fibers to 3.0, 2.5, and 2.0 eV for the doped PVP fibres with different Zn:Sn mixing ratios of 1:9, 2:8, and 3:7, respectively. This reduction can be attributed to incorporating tin ions into the polymer matrix, which introduces localized electronic states. These states reduce the energy required for electronic transitions, effectively narrowing the bandgap.

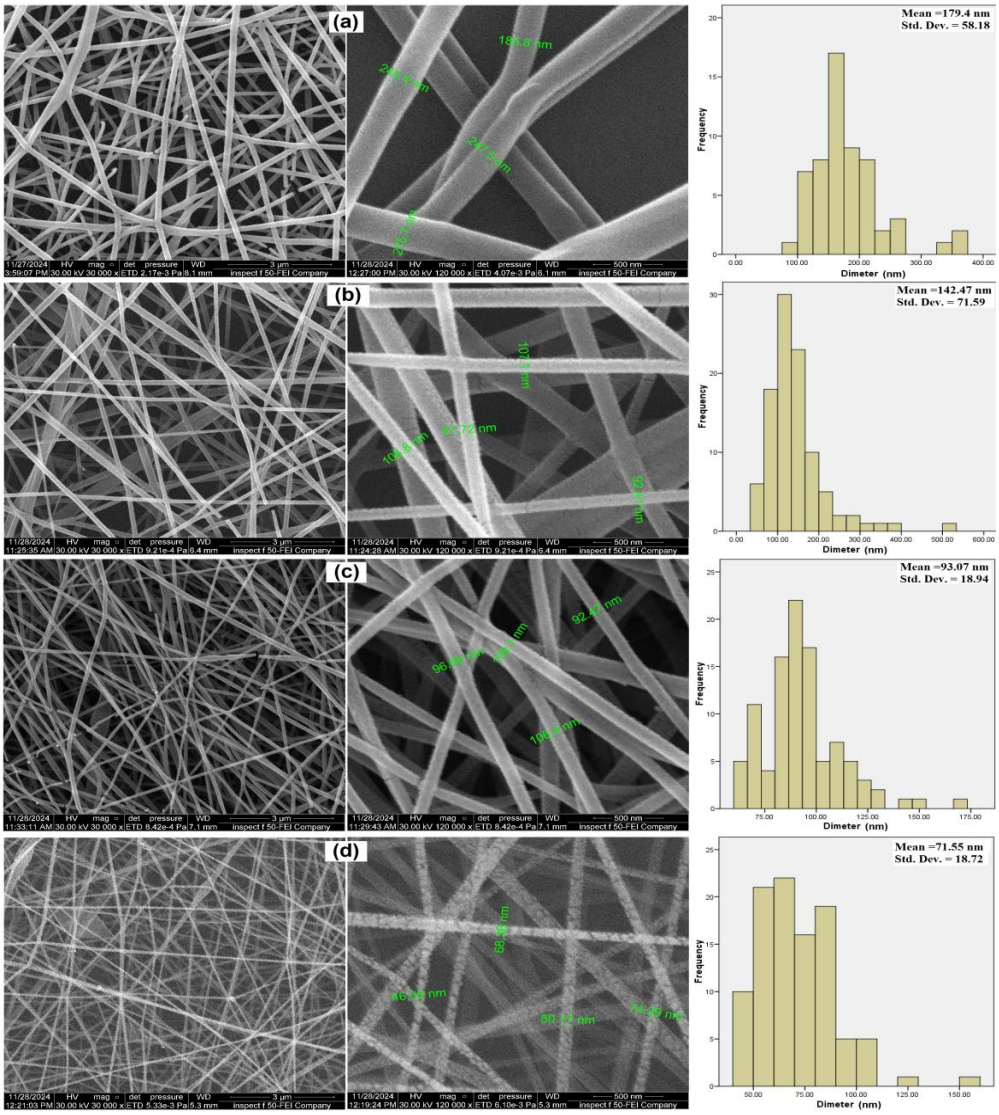


***Figure 4: FESEM images and fiber diameter distributions of (a) the electrospun PVP fiber and that of the dual doped with Zn and Sn at different mixing ratios of (b)1:9, (c) 2:8 (c), and (d)3:7.***

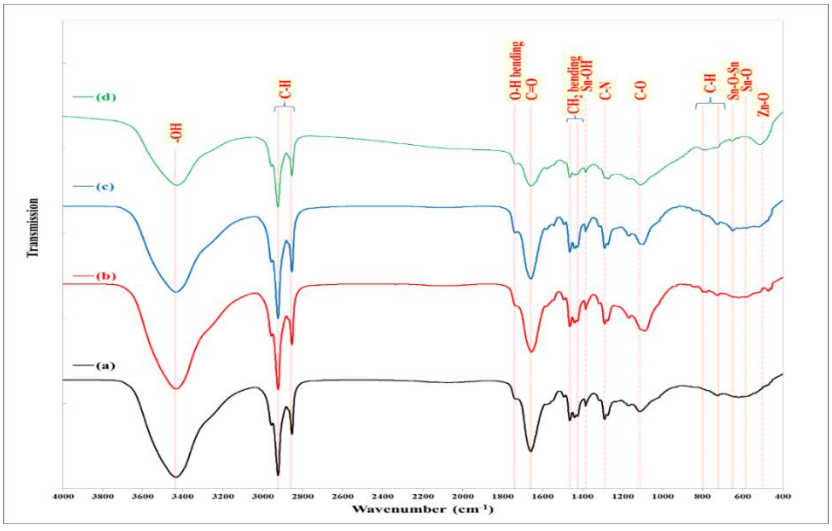


***Figure 5: FTIR of (a) the electrospun PVP fiber and that of the dual doped with Zn and Sn at different mixing ratios of (b)1:9, (c) 2:8, and (d)3:7.***

**Table 1: FTIR bands of the electrospun PVP fiber and that of the dual-doped with Zn and Sn at different mixing ratios.**

| Band Type | PVP | 1:9 | 2:8 | 3:7 |
|---|---|---|---|---|
| -OH | 3436.71 | 3431.87 | 3431.91 | 3430.87 |
| C-H stretch | 2923.22 | 2923.35 | 2923.53 | 2923.59 |
| | 2853.11 | 2853.27 | 2853.31 | 2853.33 |
| O-H bending | 1730.04 | 1730.00 | 1730.00 | 1730.00 |
| C=O | 1659.23 | 1656.93 | 1659.33 | 1658.52 |
| $CH_2$ bending | 1464.14 | 1464.25 | 1464.18 | 1464.92 |
| | 1425.07 | 1425.39 | 1425.10 | |
| Sn-OH | 1384.72 | 1384.74 | 1384.77 | 1384.82 |
| C-N | 1290.23 | 1290.00 | 1289.65 | |
| C-O | 1114.01 | 1088.13 | 1101.19 | 1113.63 |
| C-H | | 798.94 | | 792.94 |
| | 720.87 | 720.67 | 721.80 | |
| Sn-O-Sn | | | 650.21 | 651.33 |
| Sn-O | | 586.32 | | |
| Zn-O | | 456.29 | 490.00 | 490.00 |

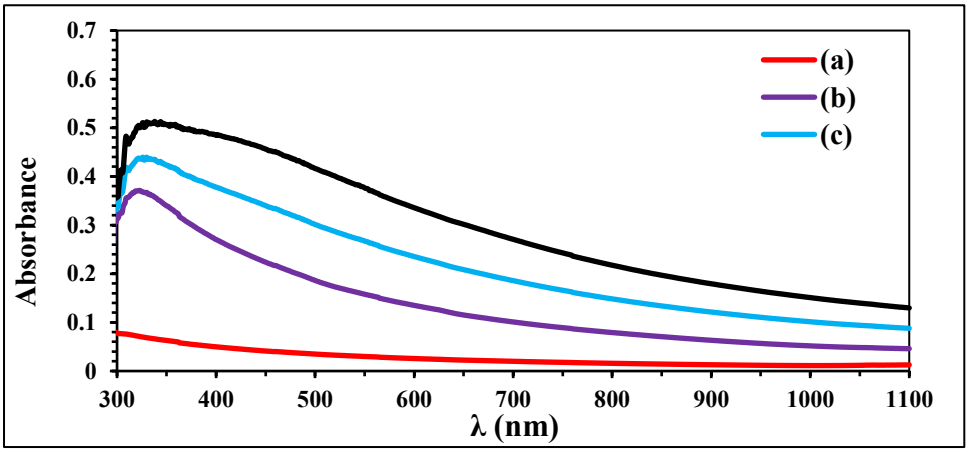


*Figure 6: UV-visible absorbance of (a)the electrospun PVP fiber and that of the dual doped with Zn and Sn at different mixing ratios of (b)1:9, (c)2:8, and (d)3:7.*

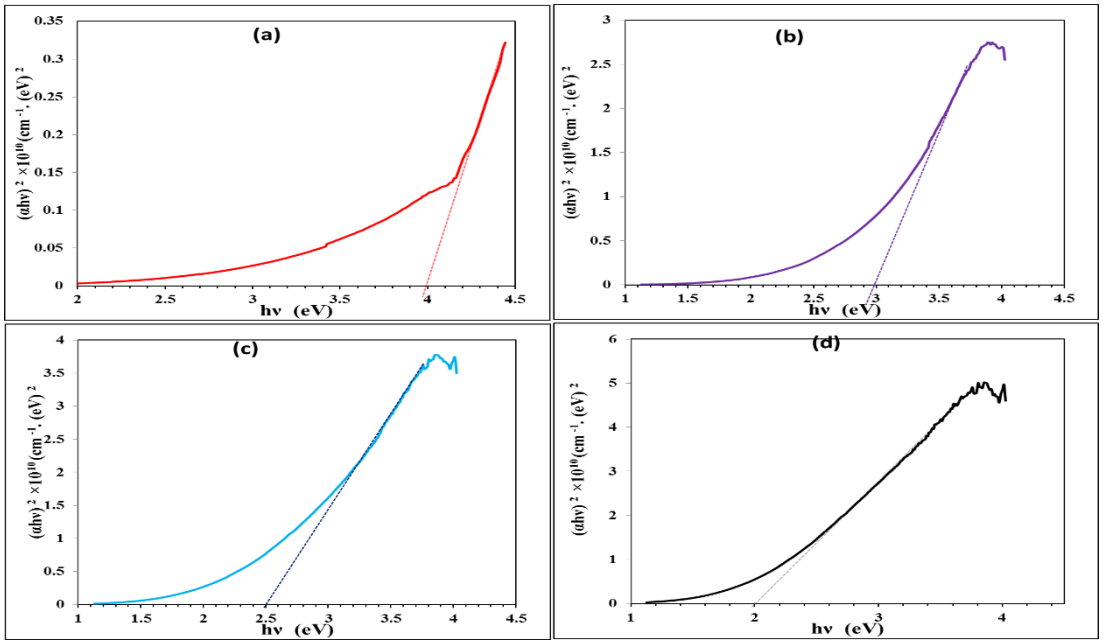


*Figure 7: Tauc plots of (a) the electrospun PVP fiber and dual doped with (Zn:Sn)ions at different ratios of (b)1:9, (c)2:8, and (d)3:7.*

Fig. 8a and b show the I-V characteristics of the pure and doped PVP fiber/n-Si photodetector systems under light and dark conditions, respectively. Both configurations exhibit a diode-like response. The light current was slightly higher than the dark current for the pure PVP fiber/n-Si photodetector. The 3:7 (Zn: Sn): PVP fiber/n-Si photodetector showed a significant increase in current under light illumination compared to the dark condition.

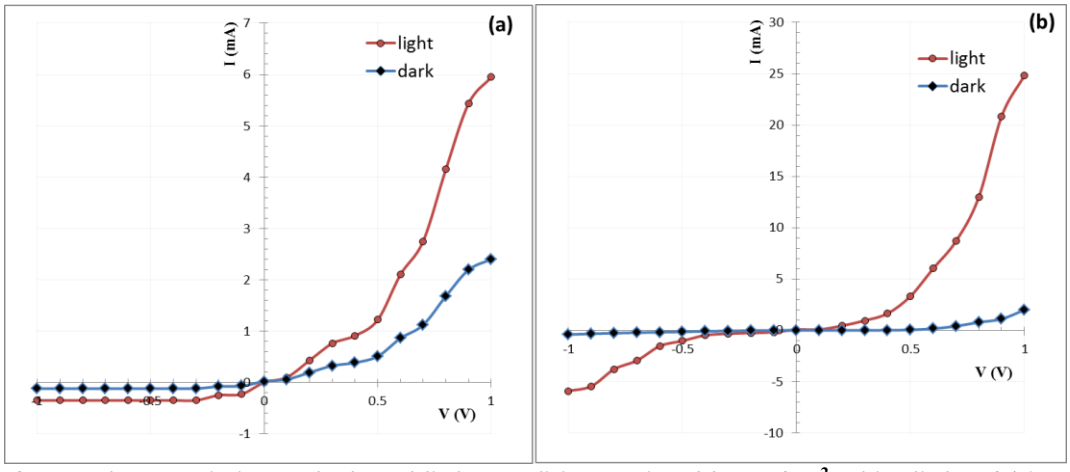


***Figure 8: I-V characteristics at dark and light conditions using 30 mW/cm$^2$ white light of (a) PVP and (b) 3:7 (Zn: Sn):PVP fiber/n-Si.***

The ideality factor (β) of the pure and doped samples was determined from the slope of the linear part at the low-bias region from the relation between ln(I) versus the applied voltages, as shown in Fig. 9.

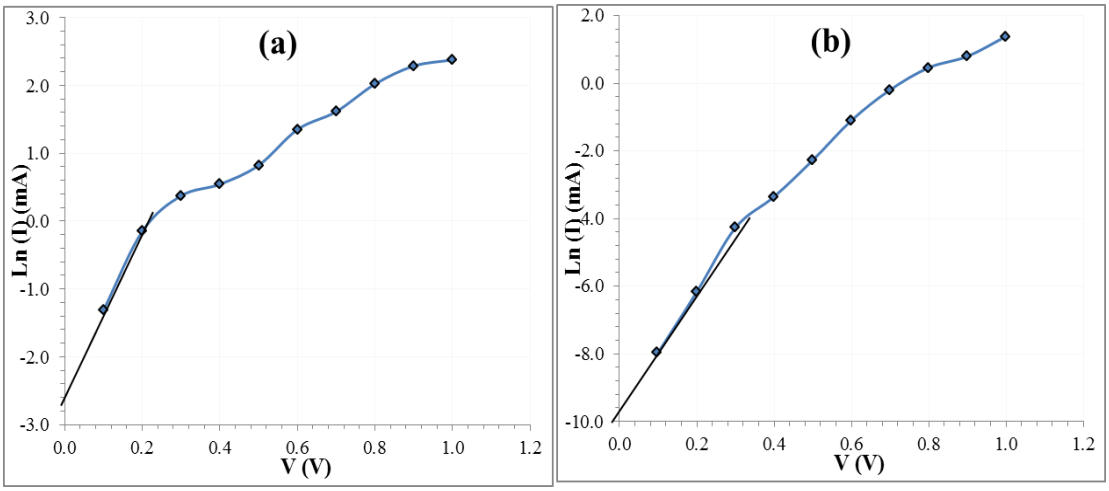


***Figure 9: (a) Ln(I) versus V of PVP fiber/n-Si (b) 3:7 (Zn, Sn ions): PVP fiber/n-Si.***

Table 2 lists a comparison between dark and light current at 1 V forward bias voltage of PVP fiber/n-Si and 3:7(Zn:Sn):PVP fiber/n-Si. The Zn and Sn dual-doped sample demonstrates significantly enhanced characteristics compared to the pure PVP fiber, where the current increased about 2.5 times that of the pure sample, and 12.4 times compared with the dark current in the doped sample. Furthermore, the ideality factor (β) of 2.15 for the doped sample was lower than that for the pure sample of 3.31, signifying better diode behavior.

**Table 2: (a) I-V characteristics parameters of PVP (b) 3:7 (Zn, Sn ions):PVP fiber/n-Si.**

| Sample | $I_{dark}$(mA) | $I_{light}$(mA) | $I_{light}/I_{dark}$ | β |
|---|---|---|---|---|
| PVP fiber/n-Si | 2.40 | 5.95 | 2.5 | 3.31 |
| 3:7 (Zn, Sn ions):PVP fiber/n-Si | 2.00 | 24.84 | 12.4 | 2.15 |

The Zn and Sn dual-doped photodetector demonstrates significantly enhanced sensitivity compared to the pure PVP fiber photodetector. The sensor of 3:7 (Zn: Sn ions):PVP fiber/n-Si was examined under different-colored light centered at 701, 609, 587, 534, 473, 422 nm wavelengths.

Fig. 10 displays the current-time (I-t) curves with light-on and –off for six colors in the visible spectrum centered at (701, 610, 587, 535, 474, and 423) nm. The curves appeared of nearly square pulses. Rise and fall times are calculated directly at a 90% variation. The sensitivity was determined according to the photocurrent ($I_{ph}$) and dark current ($I_{dark}$) using Eq. (2)[31]:

$$S\% = \frac{I_{ph}-I_{dark}}{I_{dark}} \times 100\% \quad \textbf{(2)}$$

Fig. 11 illustrates a bar graph of the photosensitivity of the fabricated photodetector fibers at a 3:7 mixing Zn:Sn ratio when illuminated with different light colors of 20 mW/cm$^2$ intensity. A variation of photosensitivity with wavelength appeared, which is attributed to differences in photon energy. Wavelengths with photon energies exceeding the bandgap induce more efficient carrier excitation, resulting in higher sensitivity. The maximum photosensitivity of 24.8% appeared at the violet light source, attributed to the adequate photon energy being higher than the calculated band gap of the active layer.

The photosensitivity variation at different light colors indicates the sample's potential as a selective photodetector for violet light. Table 3 lists the photosensitivity, rise time, and fall time at different lighting colors. Although the photon energies of red and orange light are below the estimated bandgap of the 3:7 (Zn:Sn):PVP fiber (~2.0 eV), the device still exhibits a minor measurable response. This behavior may be attributed to the introduction of localized defect states within the bandgap due to metal ion doping. These states can act as intermediate energy levels, enabling sub-bandgap photon absorption.

The fabricated (Zn,Sn):PVP/n-Si sensor achieved a violet light sensitivity of 24.8%, which is moderate when compared to the 3% La- PVP based UV photodetector, which reported a higher sensitivity of 93.75% [32], but it is significantly better than the 17.7% sensitivity observed in a previous study of 3% Ag-PVP nanofiber-based UV detector. The following equations were used to evaluate the performance of the photodetector. The quantum efficiency (η) can be calculated using the following Eq. (3) [33]:

$$\eta(\lambda) = \frac{1240}{\lambda(\mathrm{nm}) \times R_\lambda} \times 100\% \quad \textbf{(3)}$$

where λ and $R_\lambda$ represent wavelength and responsivity ($R_\lambda$), respectively.

The noise-equivalent power (NEP) is expressed in Eq. (4):

$$\mathrm{NEP} = \frac{I_n}{R_\lambda} \quad \textbf{(4)}$$

where $I_n$ is the noise current.

The Detectivity (D) and Specific Detectivity (D*) were determined according to the relations Eqs. (5 and 6):

$$D = \frac{1}{NEP} \quad \textbf{(5)}$$

$$D^* = \frac{\sqrt{\Delta f . A_d}}{NEP} \quad \textbf{(6)}$$

where $A_d$ It is an active area of the detector.

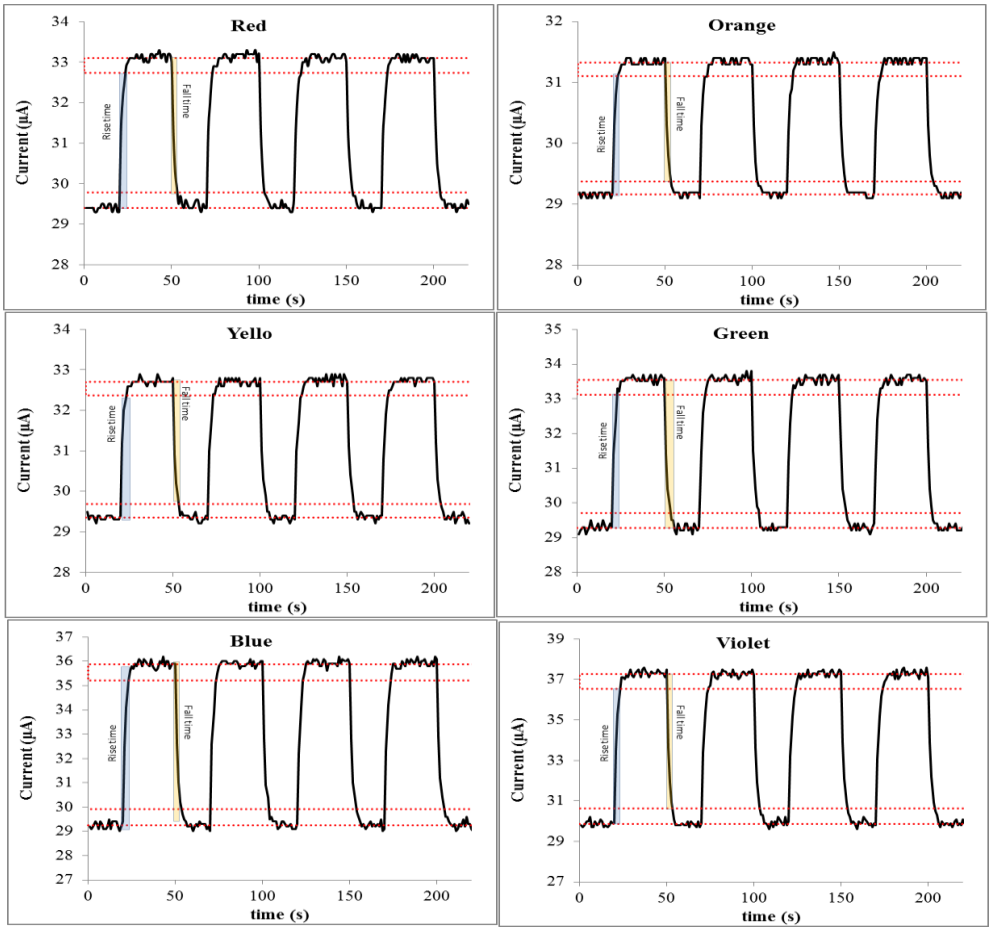


*Figure 10: Photosensitivity of the 3:7 (Zn, Sn ions):PVP fiber/n-Si using different light colors.*

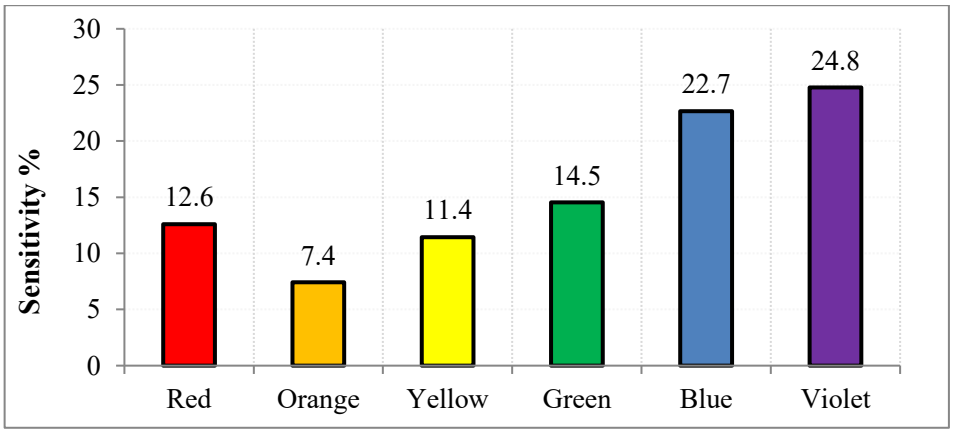


*Figure 11: Photosensitivity of 3:7 (Zn, Sn ions):PVP fiber/n-Si using different light colors.*

**Table 3: Photosensitivity, rise time, and fall time at different shining colors.**

| Color | Average λ (nm) | Sensitivity (%) | rise time (s) | Fall time (s) |
|---|---|---|---|---|
| Red | 701 | 12.6 | 3.6 | 3.6 |
| Orange | 609 | 7.4 | 3.6 | 2.9 |
| Yellow | 587 | 11.4 | 5.1 | 4.3 |
| Green | 534 | 14.5 | 2.9 | 5.1 |
| Blue | 473 | 22.7 | 4.3 | 3.6 |
| Violet | 422 | 24.8 | 2.9 | 3.6 |

Table 4 lists the detector parameters of (Zn, Sn ions):PVP fiber/n-Si across different wavelengths, including quantum efficiency, noise equivalent power, detectivity, and specific detectivity. The η values calculated according to Eq. (3) increased from 0.29% at 701 nm to a maximum of 0.55% at 422 nm, implying that the detector is more efficient at violet regions. This is consistent with the behaviour of wide-bandgap semiconductor materials. The NEP calculated based on Eq. (4) decreased from $2.90 \times 10^{-10}$ W at 609 nm to $2.44 \times 10^{-10}$ W at 422 nm, indicating improved sensitivity at shorter wavelengths. The D and D* were calculated using Eqs. (5 and 6), respectively, which are inversely proportional to NEP, decreased with decreasing wavelength.

**Table 4: η, NEP, D, and D* at different light colors.**

| Average λ (nm) | η (%) | NEP×$10^{-10}$ (W) | D ×$10^{9}$ (1/W) | D*×$10^{9}$ (cm.$Hz^{1/2}$.$W^{-1}$) |
|---|---|---|---|---|
| 701 | 0.29 | 2.74 | 3.65 | 1.27 |
| 609 | 0.32 | 2.90 | 3.45 | 1.20 |
| 587 | 0.35 | 2.78 | 3.60 | 1.25 |
| 534 | 0.39 | 2.71 | 3.69 | 1.29 |
| 473 | 0.47 | 2.53 | 3.95 | 1.38 |
| 422 | 0.55 | 2.44 | 4.11 | 1.43 |

## 4. Conclusions

This study demonstrates that electrospun PVP fibers, doped with both Zn and Sn ions, can be useful for incorporating these ions into the PVP matrix, significantly enhancing the fibers' structural, optical, and electrical properties. The dual doping also reduced fiber diameter and increased fabric density, so the active surface increased, enhancing its capability for sensing applications. The I-V characteristics of the doped fiber sensor showed enhanced photocurrent, especially under a violet light source. The doped sensor with dual doping exhibits higher current levels under illumination compared to the pure sensor. The results indicated that Zn and Sn dual doping substantially enhances the performance of PVP fiber/n-Si photodetectors, making them more suitable for advanced optoelectronic applications. The photosensitivity analysis revealed that the 3:7 sample exhibited the best performance, with a maximum sensitivity under violet light. These conclusions point to the promise of (Zn, Sn) ion-mixed PVP fibers for photodetector applications.

### Conflict of Interest

The authors declare that they have no conflict of interest.

## References

1. K.N. Narasimhamurthy, B. Daruka Prasad, B.R. Radha Krushna, S.C. Sharma, K. Ponnazhagan, D. Francis, T.B. Nijalingappa, M. Nasreen Taj, and H. Nagabhushana. Nanocomposites of PVA-PVP and l-ascorbic acid modified ZnO:Fe via ultrasonic irradiation as a green technique: Latent fingerprint detection, food packing and anti-bacterial applications, *Inorg. Chem. Commun.* **156**, 111161 (2023). https://10.1016/j.inoche.2023.111161.
2. S. Nur'aini, A. Zulfi, B.H. Arrosyid, A.F. Rafryanto, A. Noviyanto, D.A. Hapidin, D. Feriyanto, K.E. Saputro, K. Khairurrijal, and N.T. Rochman. Waste acrylonitrile butadiene styrene (ABS) incorporated with polyvinylpyrrolidone (PVP) for potential water filtration membrane, *RSC Adv.* **12**(52), 33751 (2022). https://10.1039/d2ra05969j.
3. M. Sohrabi, M. Abbasi, M.M. Ansar, and B. Soltani Tehrani. Evaluation of electrospun nanofibers fabricated using PCL/PVP and PVA/β-TCP as potential scaffolds for bone tissue engineering, *Polym. Bull.* **79**(10), 8397 (2022). https://10.1007/s00289-021-03905-5.
4. N.K. Abbas, I.M. Ibrahim, and M.A. Saleh. Characteristics of MEH-PPV/Si and MEH-PPV/PS Heterojunctions as $NO_2$ Gas Sensors, *Silicon*. **10**(4), 1345–1350 (2018). https://10.1007/s12633-017-9610-5.
5. S. Kailasa, M.S.B. Reddy, M.R. Maurya, B.G. Rani, K.V. Rao, and K.K. Sadasivuni. Electrospun Nanofibers: Materials, Synthesis Parameters, and Their Role in Sensing Applications, *Macromol. Mater. Eng.* **306**(11), 2100410 (2021). https://10.1002/mame.202100410.

6. M.S.A. Hamid and I.M. Ibrahim, Enhancement of Optoelectronic Properties of Electrospun PVA Fibers by Adding Zinc and Cobalt Ions for Photodetection Applications, *Iraqi J. Appl. Phys.* **20**(3), 687 (2024).
7. D. Ji, Y. Lin, X. Guo, B. Ramasubramanian, R. Wang, N. Radacsi, R. Jose, X. Qin, and S. Ramakrishna, Electrospinning of nanofibres, *Nat. Rev. Methods Prim.* **4**(1), 1 (2024). https://10.1038/s43586-023-00278-z.
8. I.M. Ibrahim, A.A. Safi, and N.H.M. Al-Hardan. Enhancement the sensitivity of CdS nano structure by adding of rare earth materials, in: *Journal of Physics: Conference Series,* **1178**, 012013 (2019). https://10.1088/1742-6596/1178/1/012013.
9. S. Santibenchakul, S. Chaiyasith, and W. Pecharapa, PVP-Assisted Sb-Doped $SnO_2$ Nanofibers Synthesized by Electrospinning Process, *Key Eng. Mater.* **675**–**676**, 150 (2016). https://10.4028/www.scientific.net/KEM.675-676.150.
10. M.J. Tommalieh, N.S. Awwad, H.A. Ibrahium, and A.A. Menazea. Characterization and electrical enhancement of PVP/PVA matrix doped by gold nanoparticles prepared by laser ablation, *Radiat. Phys. Chem.* **179**, 109195 (2021). https://10.1016/j.radphyschem.2020.109195.
11. S.A. Hamdan, Characterization Study of Neodymium Doped Tin Oxide Films for Optoelectronic Applications, *Iraqi J. Sci.* **65**(5), 2479 (2024). https://10.24996/ijs.2024.65.5.12.
12. S. An, H.J. Park, and M. Kim, Recent advances in single crystal narrow band-gap semiconductor nanomembranes and their flexible optoelectronic device applications: Ge, GeSn, InGaAs, and 2D materials, *J. Mater. Chem. C*, **11**(7), 2430 (2023). https://10.1039/d2tc05041b.
13. S. Zachariah, R. Indirajith, and M. Rajalakshmi, Recent advances in optoelectronic properties and applications of $Ti_3C_2Tx$ MXene, *J. Alloys Compd.* **1011**, 178296 (2025). https://10.1016/j.jallcom.2024.178296.
14. A. Qadir, S. Shafique, T. Iqbal, H. Ali, L. Xin, S. Ruibing, T. Shi, H. Xu, Y. Wang, and Z. Hu, Recent advancements in polymer-based photodetector: A comprehensive review, *Sensors Actuators A Phys.* **370**, 115267 (2024). https://10.1016/j.sna.2024.115267.
15. A.H. Alshammari, M. Alshammari, K. Alshammari, N.K. Allam, and T.A. Taha, PVC/PVP/$SrTiO_3$ polymer blend nanocomposites as potential materials for optoelectronic applications, *Results Phys.* **44**, 106173 (2023). https://10.1016/j.rinp.2022.106173.
16. J. Srivastava, P. Kumar Khanna, P. V More, and N. Singh, Chemically Synthesized Ag/PPy-PVA Polymer Nanocomposite Films As Potential EMI Shielding Material In X-band, *Adv. Mater. Lett.* **8**(1), 42 (2017). https://10.5185/amlett.2017.6486.
17. W. Jilani, A. Bouzidi, H.Y. Zahran, and I.S. Yahia, Identifying the functional properties and characterizations of PVA/PVP polymer blends incorporating CdS/ZnO core–shell (ZCS) fillers for optoelectronic applications, *J. Mater. Sci. Mater. Electron.* **35**(6), 444 (2024). https://10.1007/s10854-024-12188-1.
18. M.J. Hamadamin, N.K. Hassan, M. Humayun, and M. Bououdina, Enhancing UV light sensitivity of PVP polymer by doping chromium trioxide via the electrospun solutions, *J. Photochem. Photobiol. A Chem.* **459**, 116017 (2025). https://10.1016/j.jphotochem.2024.116017.
19. X. Zhang, Y. Yang, Z. Li, X. Liu, C. Zhang, S. Peng, J. Han, H. Zhou, J. Gou, F. Xiu, and J. Wang, Weyl Semiconductor Te/$Sb_2Se_3$ Heterostructure for Broadband Photodetection and Its Binary Photoresponse by $C_{60}$ as Charge-Regulation Medium, *Adv. Opt. Mater.* **9**(21), 1 (2021). https://10.1002/adom.202101256.
20. A. Sharma, D. Pathak, D.S. Patil, N. Dhiman, V. Bhullar, and A. Mahajan, Electrospun PVP/$TiO_2$ Nanofibers for Filtration and Possible Protection from Various Viruses like COVID-19, *Technologies.* **9**(4), 89 (2021). https://10.3390/technologies9040089.
21. C. Salma, and B.H. Rudramadevi, Spectroscopic properties of $Ho^{3+}$: PVA/PVP blend polymer films, *J. Appl. Phys.* **12**(6), 35 (2020). https://10.9790/019X-09010816.
22. W. El Hotaby, H.H.A. Sherif, B.A. Hemdan, W.A. Khalil, and S.K.H. Khalil, Assessment of in situ-Prepared Polyvinylpyrrolidone-Silver Nanocomposite for Antimicrobial Applications, *Acta Phys. Pol. A.* **131**(6), 1554 (2017). https://10.12693/APhysPolA.131.1554.
23. K. Nartetamrongsutt, and G.G. Chase, The influence of salt and solvent concentrations on electrospun polyvinylpyrrolidone fiber diameters and bead formation, *Polym.* **54**(8), 2166 (2013). https://10.1016/j.polymer.2013.02.028.
24. V. Siva, D. Vanitha, A. Murugan, A. Shameem, and S.A. Bahadur, Studies on structural and dielectric behaviour of PVA/PVP/SnO nanocomposites, *Compos. Commun.* **23**, 100597 (2021). https://10.1016/j.coco.2020.100597.
25. K. Jeyabanu, K. Sundaramahalingam, P. Devendran, A. Manikandan, and N. Nallamuthu, Effect of electrical conductivity studies for CuS nanofillers mixed magnesium ion based PVA-PVP blend polymer solid electrolyte
26. *Phys. B Condens. Matter.* **572**, 129 (2019). https://10.1016/j.physb.2019.07.049.
27. H.E. Ali, H.S.M. Abd-Rabboh, N.S. Awwad, H. Algarni, M.A. Sayed, A.F.A. El-Rehim, M.M. Abdel-Aziz, and Y. Khairy, Photoluminescence, optical limiting, and linear/nonlinear optical parameters of PVP/PVAL blend embedded with silver nitrate, *Optik*, **247**, 167863 (2021). https://10.1016/j.ijleo.2021.167863.
28. M. Teodorescu, M. Bercea, and S. Morariu, Biomaterials of PVA and PVP in medical and pharmaceutical applications: Perspectives and challenges, *Biotechnol. Adv.* **37**(1), 109 (2019). https://10.1016/j.biotechadv.2018.11.008.
29. S. Sivakumar, and E. Manikandan, Novel Synthesis of Optical, Photoluminescence Properties and Supercapacitor

Application on $Zn^{2+}$ doping $Sn_{1-x}Zn_xO_2$ nanoparticles**,** *Int. J. Sci. Res. Phys. Appl. Sci.* **6**(6), 1 (2018). https://10.26438/ijsrpas/v6i6.113.
30. Y. Pepe, Y. Tutel, S. Akkoyun, N. Asci, E. Cevik, A. Karatay, H.E. Unalan, and A. Elmali, Enhanced Nonlinear Optical Limiter in the Visible Spectral Region Based on Fe- and Co-Doped NiO Nanoparticles within PVP Nanofibers, *ACS Appl. Nano Mater.* **7**(14), 16007 (2024). https://10.1021/acsanm.4c01634.
31. R.S. Mohammed, K.A. Aadim, and K.A. Ahmed, Synthesis of CuO/ZnO and MgO/ZnO Core/Shell Nanoparticles with Plasma Jets and Study of their Structural and Optical Properties, *Karbala Int. J. Mod. Sci.* **8**(2), 88 (2022). https://10.33640/2405-609X.3225.
32. T.H. Al-Sadoon, Nanoparticles Impression on Creatine Kinase Activity, *NeuroQuantology*, **20**(1), 01 (2022). https://10.14704/nq.2022.20.1.NQ22001.
33. R.A. Ahmed, N.K. Hassan, and I.M. Ibrahim, The structural and figure of merit photodetector of PVP-doped with lanthanum, *Dig. J. Nanomater. Biostructures.* **17**(3), 759 (2022). https://10.15251/DJNB.2022.173.759.

# تأثير الخلط المزدوج لأيونات الزنك والقصدير على خصائص ألياف البولي فينيل بيروليدون المغزولة كهربائيًا لتطبيقات أجهزة الكشف الضوئية-استشعار الضوء

**ياسر عودة نايف[1] وعصام محمد ابراهيم[1]**
*[1] قسم الفيزياء، كلية العلوم، جامعة بغداد، بغداد، العراق*

## الخلاصة
تم في هذه الدراسة تصنيع ألياف بولي فينيل بيروليدون (PVP) باستخدام الغزل الكهربائي، وتم تعزيز خصائصها من خلال التطعيم المزدوج بأيونات الزنك (Zn) والقصدير (Sn). تم التحقيق في الخصائص التركيبية والبصرية والكهربائية للألياف الناتجة لتقييم إمكاناتها لتطبيقات الكاشف الضوئي. يظهر حيود الأشعة السينية لألياف PVP النقية طبيعة غير متبلورة، في حين ظهور قمتي حيود عريضتين بعد خلطها مع الأيونات بسبب المزيد من ترتيبات سلاسل PVP نتيجة لتفاعلاتها مع الأيونات المضافة. تظهر صور FESEM انخفاضًا كبيرًا في أقطار الألياف وزيادة في كثافة النسيج المحضر مع زيادة في محتوى الأيونات المعدنية. كشف تحليل FTIR عن زحزحة وتغيرات في شدة القمم المميزة وظهور نطاقات أكسيد المعدن، مما يشير إلى التفاعلات بين مصفوفة البوليمر وأيونات الشوائب، مما يساهم في تعزيز الخصائص الوظيفية. أدى دمج أيونات الزنك والقصدير إلى تحسين أداء كاشف الضوء لأجهزة ألياف PVP / n-Si بشكل كبير. نظرًا لفصل الشحنة المعزز، أظهرت العينة المشوبة زيادة بمقدار 12.5 مرة بينما فقط 2.5 مرة مقارنة بتيار الظلام في عينة ألياف PVP / n-Si النقية. أظهرت ألياف الكاشف الضوئي المصنعة بنسبة تركيب 3:7 أقصى حساسية للضوء بنسبة 24.8% تحت مصدر الأشعة البنفسجية. وتوضح نتائج هذه الدراسة إمكانات ألياف البولي فينيل بيروليدين المدمجة بأيونات الزنك والقصدير المزدوجة كمواد فعالة ومنخفضة التكلفة ومرنة لتطبيقات الكاشف الضوئي للضوء البنفسجي.

**الكلمات المفتاحية:** ألياف البولي فينيل بيروليدون، الغزل الكهربائي، كاشف ضوئي، الخصائص التركيبية، الخصائص البصرية.